frontiers | Frontiers in Earth Science

ORIGINAL RESEARCH
published: 05 May 2022
doi: 10.3389/feart.2022.891960

Sr-Nd-Hf Isotopic Disequilibrium During the Partial Melting of Metasediments: Insight From Himalayan Leucosome

Lei Yang[1,2,3], *Jia-Min Wang*[2]*, *Xiao-Chi Liu*[2], *Gautam P. Khanal*[3,4] *and Fu-Yuan Wu*[2,3]

[1]College of Earth Sciences, Chengdu University of Technology, Chengdu, China, [2]State Key Laboratory of Lithospheric Evolution, Institute of Geology and Geophysics, Chinese Academy of Sciences, Beijing, China, [3]College of Earth and Planetary Sciences, University of Chinese Academy of Sciences, Beijing, China, [4]Department of Mines and Geology, Kathmandu, Nepal

Radiogenic isotopes of granitoids are widely applied to fingerprint the source of granitoids and study the magma mingling and assimilation processes, aiming to decipher the planetary differentiation. This weapon is based on the assumption that crustal melts inherit the radiogenic isotopes of protoliths. However, complicated melting processes in the crust would drive the radiogenic isotopes of melt away from the source, thus calling for a clear understanding of the behaviors of radiogenic isotopes during crustal melting. This study investigated the joint behavior of Rb-Sr, Sm-Nd, and Lu-Hf isotope systems during the melting of metasediments. Leucosome, schist, and leucogranite samples were collected from the Nyalam, South Tibet, where the leucosome was produced by muscovite dehydration melting of metapelites. Results show that the leucosome has a broad range of Sr-Nd-Hf isotopes ($^{87}Sr/^{86}Sr_i$: 0.763,48–0.875321, $\varepsilon Nd_{(t)}$: 14.6–11.6, $\varepsilon Hf_{(t)}$: 15.0–4.4) that deviate from the metasediments. We attributed it to the non-modal or disequilibrium melting of metapelites. The variation of Sr isotopes of leucosome is formed due to preferential entry into the melt of muscovite relative to plagioclase during melting. The changing $^{87}Sr/^{86}Sri$ and $^{87}Rb/^{86}Sr$ of leucosome define an errorchron at ~ 500 Ma indicating an early Paleozoic tectono-thermal event supported by the U-Pb age of zircon cores (~460 Ma) in the leucosome. The Nd isotopes of leucosome are mainly controlled by the preferential dissolution of apatite relative to monazite. The inadequate dissolution of zircon caused more depleted initial Hf isotopes compositions in the leucosome than the source. However, the leucosome with a higher crystallization temperature has radiogenic isotopic composition closer to the source. It indicates that the melting temperature greatly affects the isotope equilibrium between source and melt.

Keywords: radiogenic isotopes, partial melting, isotope disequilibrium, leucosome, leucogranite

OPEN ACCESS

Edited by:
Tatsuki Tsujimori,
Tohoku University, Japan

Reviewed by:
Peng Gao,
Sun Yat-sen University, China
Chao Wang,
The University of Hong Kong, Hong Kong SAR, China
Feng Guo,
Guangzhou Institute of Geochemistry (CAS), China

***Correspondence:**
Jia-Min Wang
wangjm9595@gmail.com

Specialty section:
This article was submitted to Geochemistry, a section of the journal Frontiers in Earth Science

Received: *08 March 2022*
Accepted: *06 April 2022*
Published: *05 May 2022*

Citation:
Yang L, Wang J-M, Liu X-C, Khanal GP and Wu F-Y (2022) Sr-Nd-Hf Isotopic Disequilibrium During the Partial Melting of Metasediments: Insight From Himalayan Leucosome. Front. Earth Sci. 10:891960. doi: 10.3389/feart.2022.891960

1 INTRODUCTION

In the Solar System, the planetary Earth is unique in the existence of granite formed and differentiated from the partial melting of continental crust. As a powerful weapon to explore these differentiation processes, radiogenic isotopes are widely applied to fingerprint the magma source and study magma mingling and assimilation processes (DePaolo, 1981; Chappell, 1996; Wu

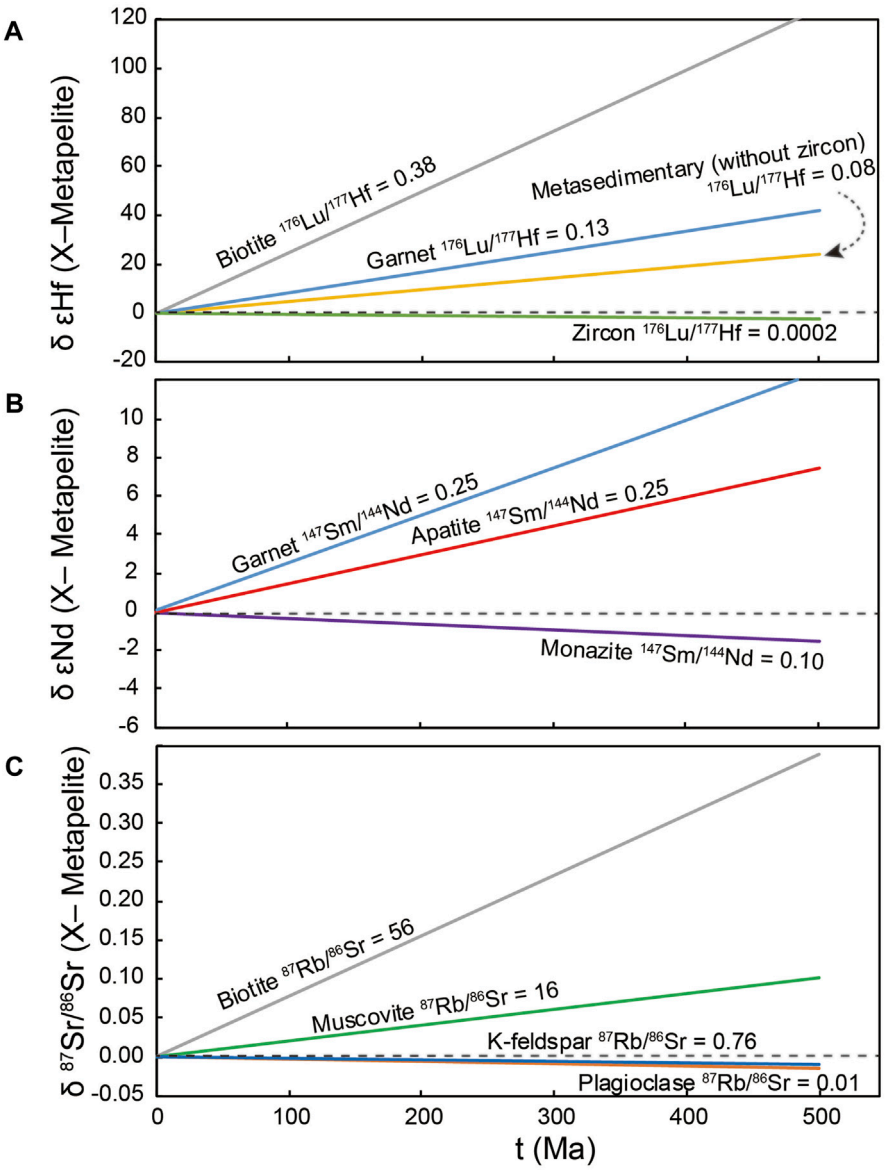

FIGURE 1 | (A) $^{87}Sr/^{86}Sr$, **(B)** εNd, and **(C)** εHf isotopic differences of rock-forming and accessory minerals in the metasedimentary rocks relative to the source due to decoupled ingrowth of radiogenic ^{87}Sr, ^{143}Nd, and ^{176}Hf. Rb, Sr, Sm, Nd, Lu and Hf concentration data are adapted from Bea et al. (1994), Faure and Mensing (2005), Zeng et al. (2005), and Rudnick and Gao (2003). Initial Sr, Nd and Hf isotopic compositions are set arbitrarily. We assumed that 90% of the Hf in the metasedimentary is in zircon.

et al., 2014). Theoretically, crustal melt should inherit the radiogenic isotopic compositions of their protoliths. However, an increasing number of studies show that non-modal melting commonly occurs during crustal melting and would deviate the radiogenic isotopes of crustal melt from the source nature (Zeng et al., 2005; Tang et al., 2014). In the source rock, constituent minerals have different parent-to-daughter ratios, and thus the elements with radiogenic ingrowth (e.g., Sr, Nd, and Hf) develop contrasting isotopic compositions with time (**Figure 1**; Wolf et al., 2019). If the isotopic differences among constituent minerals during melting onset were preserved, the melt isotopes could be determined by mineral phases entered into the melt (Knesel and Davidson, 2002; Zeng et al., 2005; Wolf et al., 2019; Xia et al., 2022). Upon the formation of melt, diffusional exchange between the melt and residue will promote isotopic equilibrium, reducing the isotopic difference between the melt and residue until they reach a balance to the source. Residue–melt isotopic equilibrium is controlled by the diffusion rates of the elements, residence time of the melt in the source, equilibrium temperature, and mineral recrystallization (Acosta-Vigil et al., 2017).

Sr, Nd, and Hf isotopes are commonly used to fingerprint the magma source. The analogous behavior of Sm-Nd and Lu-Hf isotopic systems during partial melting leads to a strong

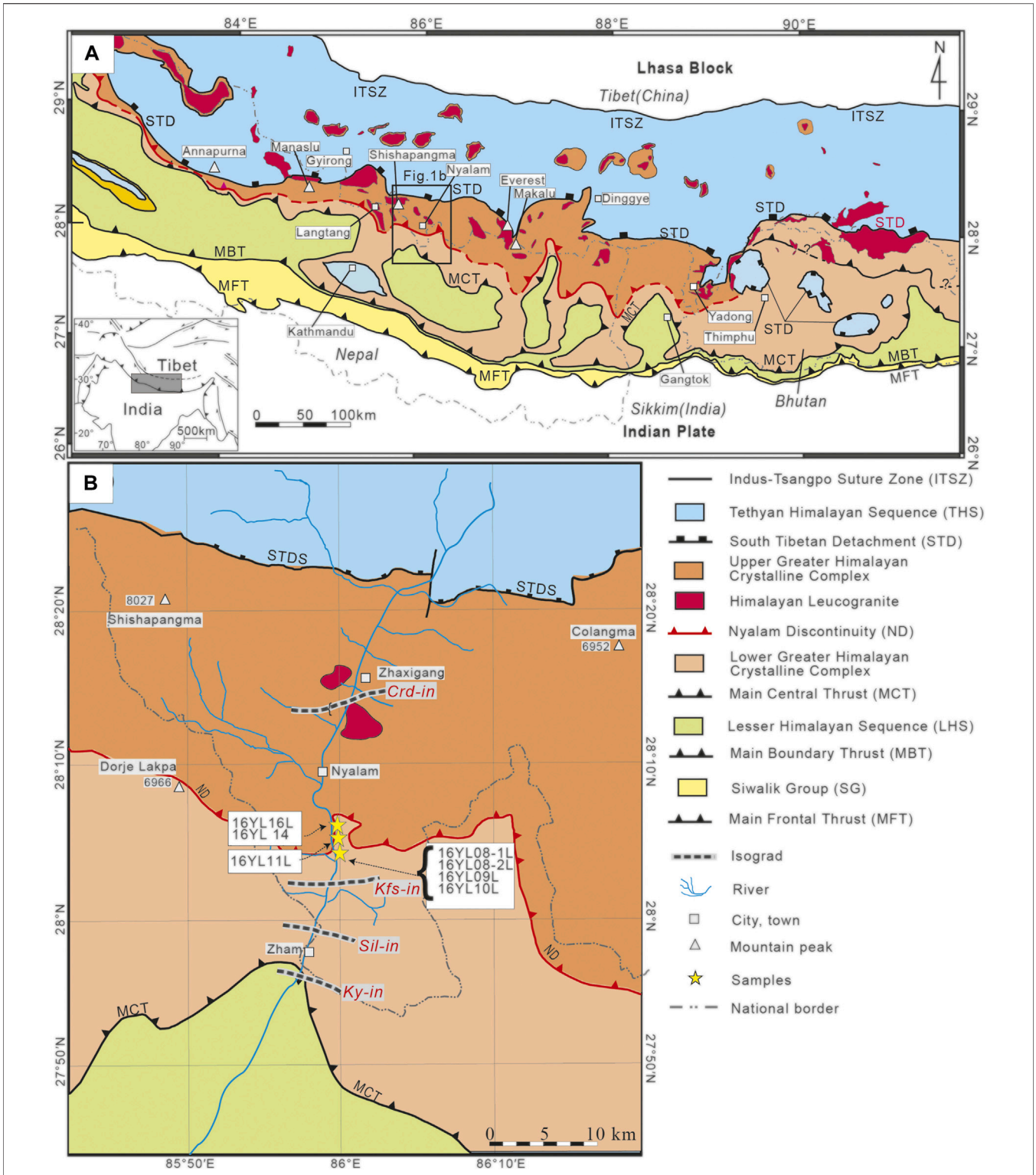

FIGURE 2 | (A) Simplified geological map showing the tectonic framework of the Himalayan orogenic belt. The rectangle indicates the location of the Nyalam. **(B)** Geological sketch map of the Nyalam region (modified after Wang et al., 2015). Mineral abbreviations follow Whitney and Evans (2010).

correlation of the Nd-Hf isotopes that should lie in the Terrestrial Array (Vervoort et al., 2011). Nearly all terrestrial rocks from various sources commonly negative correlates between $^{87}Sr/^{86}Sr$ and $^{143}Nd/^{144}Nd$ isotopic ratios (Clemens et al., 2017). Therefore, the Sr-Nd-Hf isotopes are usually coupled in the crustal rocks. The occurrence of isotopic signatures that deviate from this

coupling relationship is thought to be associated with the non-modal or disequilibrium melting processes (Zeng et al., 2005; Zhang et al., 2020). Many studies have identified the isotopic disequilibrium of Sr and Nd during anatexis of metasediments (Knesel and Davidson, 2002; Zeng et al., 2005; Wolf et al., 2019). However, Hf isotopic disequilibrium is mainly found in granitic pluton and is evidenced by modeling (Farina et al., 2014; Tang et al., 2014; Zhang et al., 2020). A reasonable explanation of the anomaly between Sr, Nd, and Hf depends on a clear understanding of the joint behavior of the Sr-Nd-Hf isotopic systems during anatexis of metasediments.

Migmatites, a product of crustal anatexis (Weinberg, 2016), commonly trap *in situ* melt from the source of partial melting and offer an opportunity to study the Sr-Nd-Hf variations during crustal anatexis. In the Himalayas, migmatites are widely exposed, and leucosome within the migmatite is produced by anatectic melting of metasediments (Wang et al., 2015; Wang et al., 2017), making it an ideal material to study the joint behavior of Sr-Nd-Hf isotopic systems during crustal partial melting. This work collected schist, leucosome, and leucogranite from the Great Himalayan Crystalline (GHC) in Nyalam and analyzed their whole-rock Sr-Nd-Hf isotopes. Our work proved that the muscovite dehydration melting reactions and incomplete dissolutions of accessory phases during low-degree partial melting resulted in the deviation of Sr-Nd-Hf isotopes between the melt and the source and their deviation from the array of terrestrial rocks.

2 GEOLOGICAL CONTEXT AND PETROLOGY

The Himalayan orogenic belt in southern Tibet resulted from the India-Asia collision along the Indus–Tsangpo suture zone (Najman et al., 2010). The Indian plate can be divided into the Tethyan Himalayan Sequence (THS), the GHC, and the Lesser Himalayan Series (LHS) from north to south. They were bounded by the Southern Tibetan detachment system (STDS) and the Main Central Thrust (MCT). The GHC consists of late Proterozoic to early Cambrian metasedimentary rocks, which were experienced amphibolite to granulite facies metamorphism. It was intruded by numerous Cambrian–Ordovician plutons (**Figure 2A**).

Nyalam is located in the central Himalaya, southern Tibet, with Shishapangma to the north, Manaslu to the west, and Langtang to the east (**Figure 2B**). The Nyalam Valley is famous for the birth of the concept of Southern Tibet Detachment (Burchfiel et al., 1992) and excellent exposures of the migmatites, leucosome, and leucogranite within the GHC (Wang et al., 2013; Wang et al., 2015; Leloup et al., 2015; Yang et al., 2019). The leucogranite in the Nyalam occurs as sill, small laccolith, and dyke, which was emplaced during Miocene time (27–14 Ma; Yang et al., 2019). Within the GHC, the metamorphic grade increases gradually, indicated by key index metamorphic minerals change from chlorite, garnet, to staurolite in the LHS, and kyanite, sillimanite–muscovite, sillimanite–K-feldspar, and cordierite in the GHC (Wang et al., 2013; Yang et al., 2019). Geothermobarometry data showed that the minimum peak temperature gradually increases from ~580°C in the upper LHS to ~750°C in the upper GHC, whereas metamorphic pressure decreases from 1.0–1.3 to 0.4–0.7 GPa (Wang et al., 2013). Within the sillimanite–K-feldspar zone of the GHC, the internal tectono-metamorphic discontinuity (Nyalam Discontinuity) divides the GHC into lower and upper subunits, with younger ages toward the foreland of the orogenic wedge, forming a duplex structure within the GHC (Wang et al., 2015, 2016). Migmatites are widely distributed in the sillimanite–K-feldspar zone in the middle and upper GHC, where abundant leucosome has been reported with major and trace elements (Yang et al., 2019). In general, leucosome occurs as light-colored layers within stromatic metatexite in the migmatitic paragneiss and orthogneiss. They were produced by muscovite dehydration melting of metasediments according to the petrography, P-T conditions, and geochemistry (Wang et al., 2013; Wang et al., 2015; Yang et al., 2019). Above the cordierite zone, *in situ* leucosome is rare.

In this study, six leucosome samples were separated manually and processed for whole-rock Sr-Nd-Hf isotopic analysis and zircon U-(Th)-Pb dating. The samples were collected mainly from the migmatites of sillimanite–K-feldspar zone around the Nyalam Discontinuity (**Figure 2B**). The migmatite is stromatic metatexite containing centimeter-to decimeter-scale leucosome. Field investigations confirmed that the leucosome is *in situ* (**Figure 3A,B**). The centimeter-scale, layer-parallel leucosome can be traced to their anatectic protoliths. The leucosome has a granoblastic texture and consists of quartz (~30%), K-feldspar (~40%), plagioclase (~20%), biotite (~4%), sillimanite (~3%), garnet (~2%), and accessory (~1%) zircon, monazite, and apatite. In general, the quartz, K-feldspar, and plagioclase are much coarser than in mesosomes or melanosomes. Trace amounts of resorbed muscovite are found in or adjacent to the leucosome, consistent with the formation of K-feldspar and sillimanite during anatexis (**Figures 3D–G**). The melanosomes are composed of alternating layers of sillimanite, biotite, K-feldspar, plagioclase, and ilmenite (**Figure 3G**). The biotite contains numerous inclusions of accessory minerals, e.g., monazite (**Figure 3H**). Monazite U–(Th)–Pb dating indicates that the leucosome was crystallized during 16–14 Ma (Yang et al., 2019). The detailed location and whole-rock geochemistry of the leucosome have been reported in Yang et al. (2019). The schist sample (16YL14) was collected in the sillimanite–K-feldspar zone, a few meters away from sample 16YL12 (GPS: N28°07′02″, E85°59′43″). It consists of quartz (50%), plagioclase (30%), k-feldspar (10%), and biotite (10%). Field and petrographic observations have shown that the schist has not experienced migmatization. We assumed that it represents the protolith corresponding to the leucosome.

The 32 leucogranite samples were collected along a North-South transect across the GHC in Nyalam, from varying occurrences as dikes, sills, and plutons (**Figure 3C**). Like other

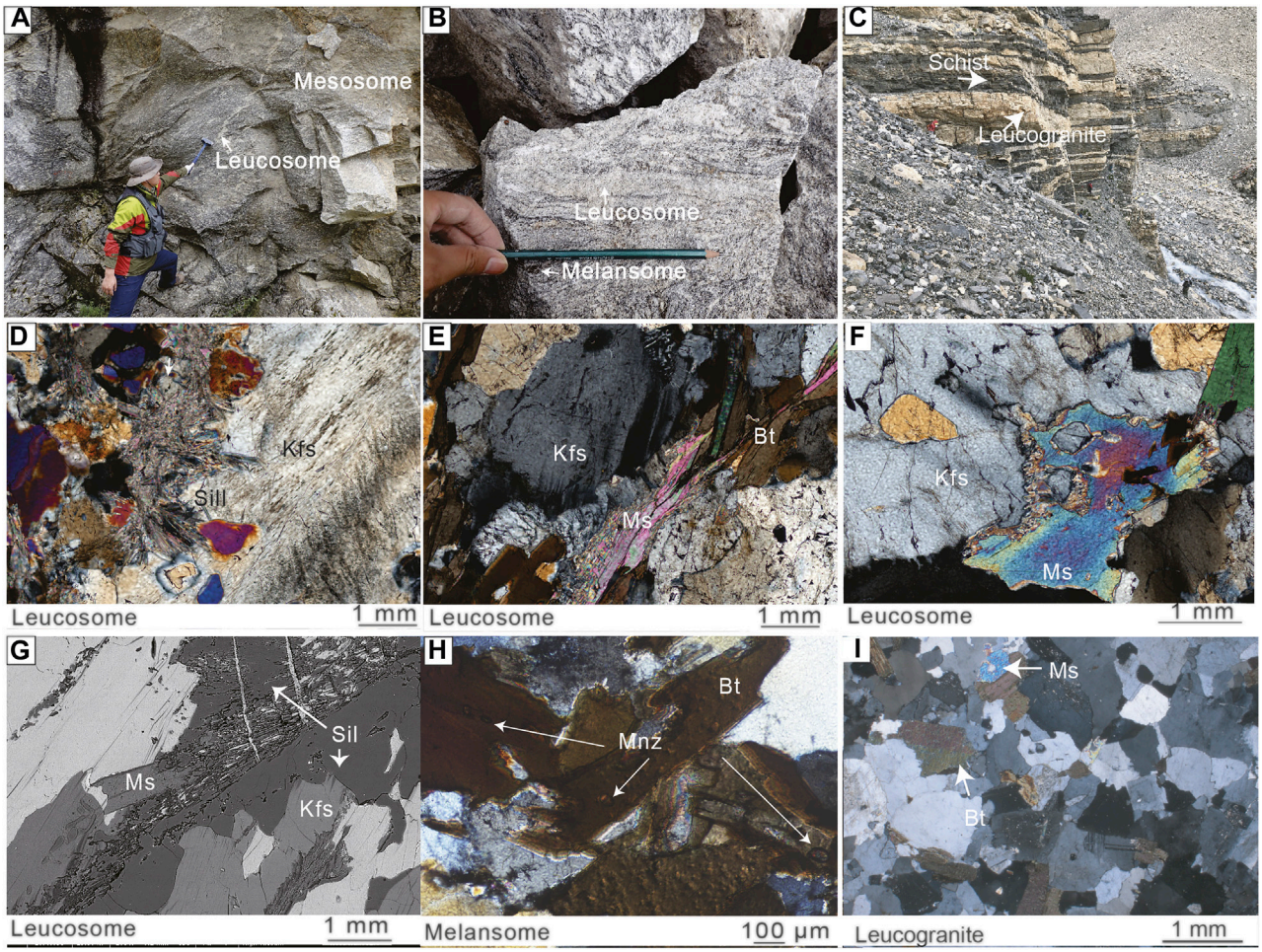

FIGURE 3 | (A and B) Representative outcrop photographs of the leucosome, **(C)** and leucogranite in the Nyalam region. **(D and F)** Microphotographs of leucosome showing the muscovite dehydration melting reactions defined by Ms relicts adjacent to the Kfs and Sil. **(G)** Back-scattered electron image of leucosome showing the muscovite dehydration melting reactions. **(H)** Monazite were wrapped in the biotite of the melansome. **(I)** Microphotographs of the leucogranite..

Himalayan leucogranite (Wu et al., 2020), the principal minerals of the Nyalam leucogranite are quartz, plagioclase, and K-feldspar, with minor varietal muscovite, tourmaline, biotite, and garnet (**Figure 3I**). Principle accessory minerals are zircon, monazite, apatite, and xenotime. Chloritization and sericitization have affected biotite and plagioclase in some leucogranites.

3 ANALYSIS METHOD

3.1 U–(Th)–Pb Zircon Analysis

Zircon laser ablation (LA)–ICP–MS U–(Th)–Pb dating was conducted with an Agilent 7500a quadrupole ICP–MS coupled to a 193-nm excimer laser ablation system. Detailed analytical procedures are provided by Xie et al. (2008). The $^{207}Pb/^{206}$ Pb, $^{206}Pb/^{238}U$, $^{207}U/^{235}U$ (^{235}U = $^{238}U/137.88$), and $^{208}Pb/^{232}Th$ ratios were corrected using zircon 91,500 as an external standard. The fractionation correction and results were calculated using GLITTER 4.0 (GEMOC, Macquarie University; Griffin et al., 2008). The U–(Th)–Pb dating of standard samples is given in **Supplementary Table S1**.

3.2 Whole-Rock Sr-Nd-Hf Isotope Analysis

High precision isotopic (Sr, Nd, and Hf) measurements were carried out at Nanjing FocuMS Technology Co., Ltd. Geological rock powders were mixed with 60 wt% HNO_3 (0.5 ml) and 40 wt% HF (1.0 ml) in high-pressure PTFE bombs. These bombs were steel-jacketed and placed in the oven at 195°C for 3 days. Digested samples were dried down on a hotplate and reconstituted in a 1.5-ml of 1.5 N HCl before ion exchange purification. The detail of the purification processes of Sr, Nd, and Hf was reported by Ji et al. (2020). Diluted solutions (50 ppb Sr, 50 ppb Nd, and 40 ppb Hf) were introduced into Nu Instruments Nu Plasma II MC–ICP–MS. Raw data of isotopic ratios were internally corrected for mass fractionation by normalizing to $^{86}Sr/^{88}Sr = 0.1194$ for Sr, $^{146}Nd/^{144}Nd = 0.7219$ for Nd, and $^{179}Hf/^{177}Hf = 0.7325$ for Hf with exponential law. International isotopic standards (NIST SRM 987 for Sr, JNdi-1 for Nd, Alfa Hf) were periodically analyzed to correct instrumental drift. Geochemical

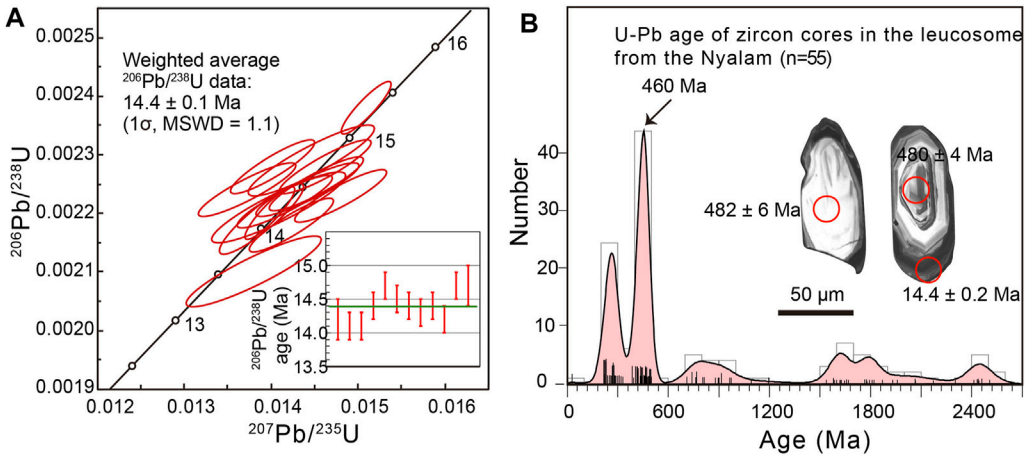

FIGURE 4 | (A) The U–(Th)–Pb dating of zircon rims in the leucosome **(B)** The kernel density estimates of zircon cores ^{207} Pb/^{235}U ages in the leucosome. Inserted images show the represented zircons from the leucosome. The red circle is the laser spot. The data are listed in **Supplementary Table S3**.

reference materials of USGS BCR-2, BHVO-2, AVG-2, RGM-2, and W-2 were treated as quality control. The isotopic compositions of standard samples are given in **Supplementary Table S2**. The values agreed with previous publications within analytical uncertainty (Weis et al., 2006, 2007).

4 RESULT

4.1 U–(Th)–Pb Geochronology of Inherited Zircons

Zircons extracted from the leucosome samples are 100–200 μm in size. Cathodoluminescence (CL) imaging of the zircon internal structures shows euhedral, oscillatory zoned core domains, which are truncated and overgrown by broad, faintly oscillatory zoned rim domains (**Figure 4B**). LA–ICP–MS analyses of the zircon rim domains show lower Th/U ratios relative to the core (rim domains: Th/U = 0.01–0.02; core domains: Th/U = 0.01–1.8). These data are between 95 and 110% concordant. Fourteen spot analyses of the rim yield an age of 14.4 ± 0.1 Ma (1σ; MSWD = 1.1), represent the time of crystallization time (**Figure 4A**). Fifty-five spot analyses of the cores were performed. Except two spots have the age older than Neoproterozoic time, others display scattered ages ranging from 895 ± 10 Ma to 147 ± 1 Ma (^{207}Pb/^{235}U ages with one sigma, **Figure 4B**), which precludes a single-weighted mean age from being calculated. The kernel density estimates (KDE) present a primary age peak at ~460 Ma (**Figure 4B**). The analyses data are shown in **Supplementary Table S3**.

4.2 Whole-Rock Radiogenic Isotopes

The Sr-Nd-Hf isotopes of the leucosome, schist, and leucogranite in this study were listed in **Supplementary Table S4** and plotted in **Figures 5**, **6**. Measured ^{87}Sr/^{86}Sr ratios of leucosome range between 0.764503 ± 5 and 0.879092 ± 3 and the recalculated initial ^{87}Sr/^{86}Sr$_i$ (for ages of each sample were reported by Yang et al. (2019), t = 16–14 Ma) range between 0.763248 ± 4 and 0.875321 ± 3 (**Figures 5A,B**). The initial Sr isotopic composition is correlated with Sr content variation and Rb/Sr ratio (**Figures 5A,B**). In addition, it defines a crude ~500 Ma errorchron with the ^{87}Rb/^{86}Sr ratio, which is consistent with the trend that appears in the Langtang migmatite (**Figure 5B**; Harris and Ayres, 1998). One schist sample from Nyalam has the ^{87}Sr/^{86}Sr ratio 0.729312 and recalculated ^{87}Sr/^{86}Sr$_i$ (t = 15 Ma) ratio 0.729029. Measured ^{87}Sr/^{86}Sr ratios of leucogranite range between 0.744519 ± 5 and 0.771546 ± 4, and recalculated initial ^{87}Sr/^{86}Sr$_i$ range between 0.737481 ± 4 and 0.765985 ± 3 (t = 15 Ma).

Measured ^{143}Nd/^{144}Nd isotopes of leucosome range between 0.511884 ± 4 and 0.512044 ± 5, and recalculated initial $\varepsilon Nd_{(t)}$ range between −11.6 and −14.6 (**Figure 5C**). A remarkable feature is that their initial Sr and Nd isotopic compositions show a positive relationship (**Figure 5D**). The schist from the Nyalam has the ^{143}Nd/^{144}Nd ratio 0.511690 and recalculated $\varepsilon Nd_{(t)}$ (t = 15 Ma) of −18.3. Measured ^{143}Nd/^{144}Nd isotopes of leucogranite range between 0.511817 ± 6 and 0.511912 ± 2, and recalculated initial $\varepsilon Nd_{(t)}$ range between −16.1 and −14.0 (t = 15 Ma).

The measured ^{176}Hf/^{177}Hf isotopes of leucosome range from 0.282350 ± 3 to 0.282654 ± 3. The recalculated initial $\varepsilon Hf_{(t)}$ range between −4.4 and −15.0 (**Figure 6A**). The Hf-Nd isotopes are positively correlated (**Figure 6B**). The schist sample from the Nyalam has the ^{176}Hf/^{177}Hf ratio 0.281965 and recalculated $\varepsilon Nd_{(t)}$ (t = 15 Ma) of −28.7. Measured ^{176}Hf/^{177}Hf isotopes of leucogranite range from 0.282386 ± 2 to 0.282190 ± 2. The recalculated initial $\varepsilon Hf_{(t)}$ range between −13.3 and −20.3 (t = 15 Ma).

5 DISCUSSION

5.1 The Record of the Early Paleozoic Tectono-Thermal Events

Pre-Himalayan evolution is essential to rebuilding the supercontinents (e.g., Gondwana assemblage; Cawood et al., 2007). However, it is much harder to decipher due to this pervasive Cenozoic metamorphic overprint (Palin et al., 2018). In

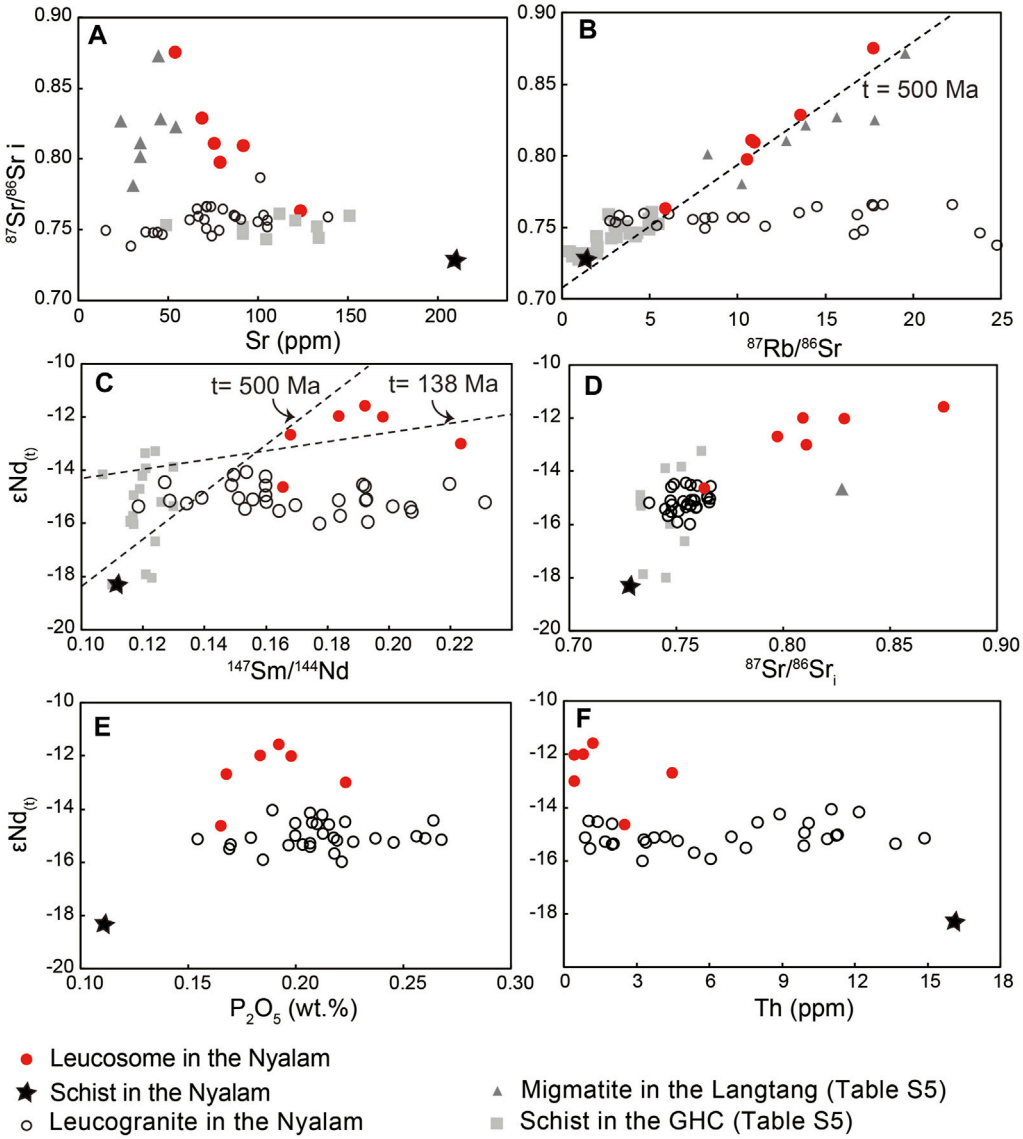

FIGURE 5 | Plots of $^{87}Sr/^{86}Sri$ vs. **(A)** Sr content, **(B)** $^{87}Rb/^{86}Sr$ ratios, and εNd(t) vs. **(C)** $^{147}Sm/^{144}Nd$ ratio, **(D)** $^{87}Sr/^{86}Sr_i$ ratio, **(E)** P_2O_5 content, and **(F)** Th content for the Nyalam leucosome, leucogranite, and schist in this study, migmatites in the Langtang (Inger and Harris, 1993), and schists in the GHC (Deniel et al., 1987; Inger and Harris, 1993; Parrish and Hodges, 1996; Robinson et al., 2001). The literature data are listed in **Supplementary Table S5**. The $^{87}Sr/^{86}Sr_i$ and $εNd_{(t)}$ values of the leucosome and leucogranite are calculated by their crystallization ages reported in Yang et al. (2019). Others are corrected to 15 Ma. The dashed lines in the **(B)** and **(C)** indicate the 500 Ma and 138 Ma errorchrons.

this study, analyses of the zircon rim of leucosome yield an age of 14.4 ± 0.1 Ma, consistent with the monazite age reported by Yang et al. (2019). We suggest that this age represents the timing when anatectic melt crystallization. In the projection of $^{87}Rb/^{86}Sr$ versus $^{87}Sr/^{86}Sr_i$, the errorchron is distributed around ~500 Ma. In addition, inherited zircon cores in the leucosome yield a prominent age peak at ~460 Ma (**Figure 4B**). Similar errorchron age in the migmatite was reported by Inger and Harris (1993) from the Langtang to the east of Nyalam. Although such crude "age" has a large uncertainty, it indicates the timing that the GHC were partially homogenized with concerning Sr isotopes (Inger and Harris, 1993). From the Neoproterozoic to early Paleozoic, the GHC is in the northern margin of Gondwana and has experienced a series of orogenic events along with the Andean-type subduction (Cawood et al., 2007). The Cadomian orogeny lasted from ~650 to ~540 Ma (Linnemann et al., 2014; Gao et al., 2019), followed by the ~510–460 Ma Ordovician Bhimpedian (or Kurgiakh) orogeny (Myrow et al., 2006; Cawood et al., 2007), which is most closely related to the age recorded in the leucosome. This early Paleozoic orogeny was accompanied by widespread granitoid magmatism, now exposed in GHC and North Himalayan Gneiss domes aged 520–460 Ma (DeCelles et al., 2000; Cawood et al., 2007; Wang et al., 2012; Gao et al., 2019) and high-grade metamorphism (Cawood et al., 2007; Palin et al., 2018).

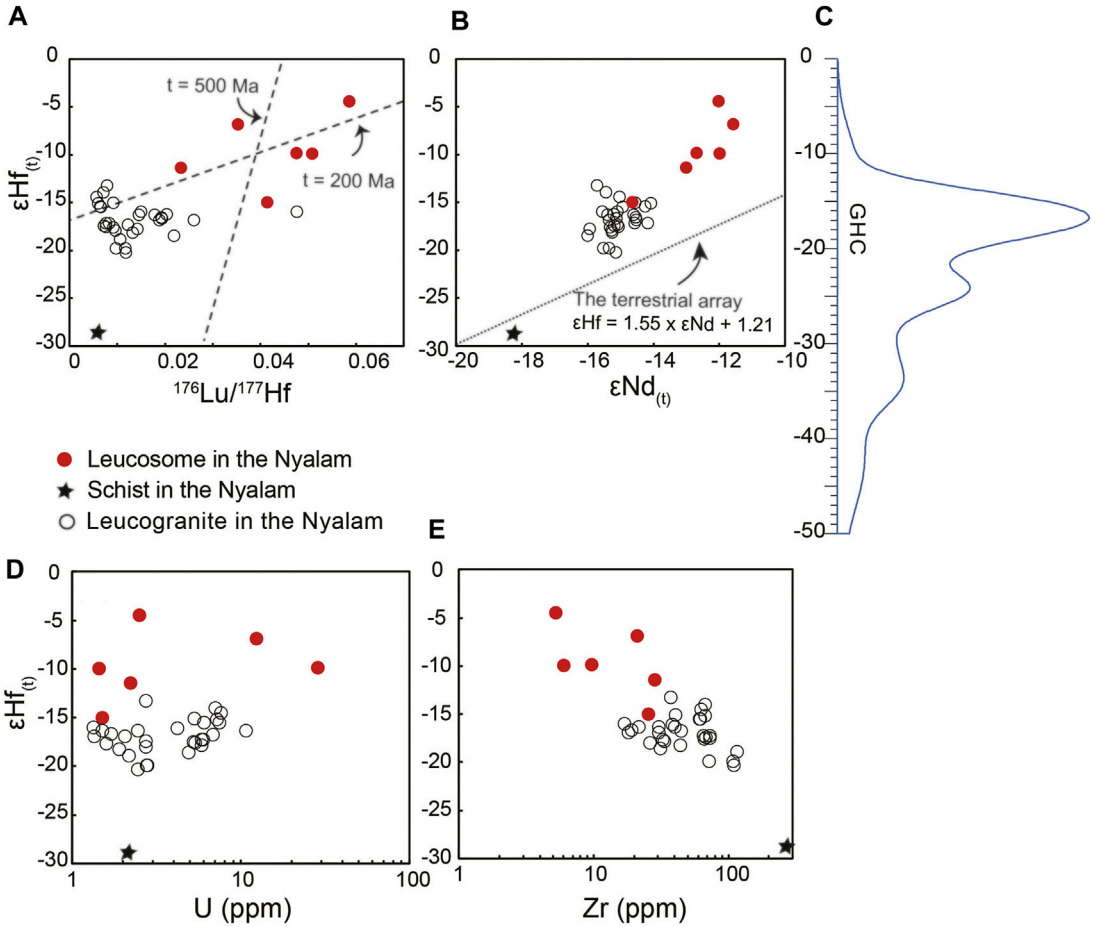

FIGURE 6 | Plots of $\varepsilon Hf_{(t)}$ vs. **(A)** $^{176}Lu/^{177}Hf$, **(B)** $\varepsilon Nd_{(t)}$, **(D)** U, and **(E)** Zr for the leucosome, schist, and leucogranite in the Nyalam. The dashed lines in the **(A)** indicate the 500 Ma and 200 Ma errorchrons. The dotted line in the **(B)** shows the terrestrial array regressed by Vervoort et al. (2011). **(C)** The kernel density estimates of the GHC (Langtang) detrital zircon data, recalculated at 15 Ma, based on the composition of Spencer et al. (2019) (**Supplementary Table S5**).

Unlike the Rb-Sr isotopic system, the Sm-Nd and Lu-Hf isotopic systems in the leucosome present errorchron ages of ~138 Ma and ~200 Ma, respectively (**Figures 5C**, **6A**). Such Mesozoic ages are unlikely to be related to any tectonic event because there is no record of Mesozoic metamorphism in the Himalayan orogenic belt (Kapp and DeCelles, 2019). We suggest that these errorchron ages record partially resetting intermediate ages. The absence of early Paleozoic ages in the Sm-Nd and Lu-Hf isotopic systems is perhaps due to the small ranges in $^{147}Sm/^{144}Nd$ and $^{176}Lu/^{177}Hf$ values and variability in the initial Nd and Hf isotopic ratios. The samples in this study were collected from tens of meters to a few kilometers in spatial distance, placing a maximum constraint on the length scale of isotopic re-equilibration during the Himalayan metamorphism.

5.2 The Sr-Nd-Hf Isotopic Disequilibrium of the Leucosome

Enriched $^{87}Sr/^{86}Sr_i$, $\varepsilon Nd_{(t)}$, and $\varepsilon Hf_{(t)}$ compositions in the leucosome indicate its typical crustal origin (**Figures 5**, **6**). It is consistent with that the leucosome in this study was produced by muscovite dehydration melting of the GHC metasediments (Yang et al., 2019) However, the leucosome has a broad range of Sr-Nd-Hf isotopes. The origin of the isotopic variability is usually explained in two perspectives: 1) magma mingling and assimilation (DePaolo, 1981; Chappell, 1996); 2) varied crustal sources (Ji et al., 2022); and 3) the isotopic heterogeneity in the source (Deniel et al., 1987). We preclude the first and second assumptions because the leucosome is *in situ* or in-source melt in this study. To discuss the third possibility, we compiled the Sr-Nd-Hf isotopic data of the GHC (**Supplementary Table S5**; Deniel et al., 1987; Inger and Harris, 1993; Parrish and Hodges, 1996; Robinson et al., 2001; Spencer et al., 2019). The compiled data are age-corrected to 15 Ma, the timing of leucosome crystallization. The whole-rock Sr-Nd isotopic data from Manaslu and Langtang show that the GHC has $^{87}Sr/^{86}Sr_i$ from 0.73 to 0.76, and $\varepsilon Nd_{(t)}$ from −15 to −20 (**Figures 5A,B**). The zircon Hf isotopic data from Spence et al. (2019) show that the GHC in the Langtang has $\varepsilon Hf_{(t)}$ values from −8 to −18 (**Figure 6C**). In this study, the schist in the Nyalam has semblable isotopic compositions as those reported in

the literature. A remarkable feature of the leucosome is that the Sr-Nd-Hf isotopic compositions deviate in varying degrees from the GHC migmatites (**Figures 5**, **6**). The leucosome yields more radiogenic Sr isotopes composition and less radiogenic Nd and Hf isotopes than the GHC metasediments. It implies that the Nyalam leucosome does not inherit the source isotopic signature of the source, and another process may have driven the isotopes of melt away from the source.

Partial melting in natural rocks always occurs in open systems. The composition of anatectic melts might be affected by melt lost or fractional crystallization, addition of restite, and reverse reaction between melt and restite (Taylor et al., 2014; Brown et al., 2016). Yang et al. (2019) performed detail petrographic and geochemical work to the leucosome in this study, and suggested that the composition of leucosome might be affected by fractionation crystallization and disequilibrium melting. However, it is difficult for the fractional crystallization to affect the isotopic composition of leucosome. For the radiogenic elements, isotopic fractionations are negligible and do not change the isotopes of the melt from the source and crystallized minerals. Another possible process might be non-modal melting or disequilibrium melting (Zeng et al., 2005; Tang et al., 2014; Wolf et al., 2019). Knesel and Davidson (2002) suggested that the various $^{87}Sr/^{86}Sr$ ratios in the melt showed a range of values depending on the mineral phase involved in the melting process. Higher Rb/Sr ratio in the muscovite results in a radiogenic $^{87}Sr/^{86}Sr$, rather than a lower Rb/Sr ratio and unradiogenic $^{87}Sr/^{86}Sr$ in the plagioclase (Knesel and Davidson, 2002). In our study, leucosomes were produced by muscovite dehydration melting (Wang et al., 2013, 2015; Yang et al., 2019), with possible reaction as followings (Patiño Douce and Harris, 1998):

$$22Mus + 7Pl + 8Qz \rightarrow 5Kfs + 5Sill + 2Bt + 25L \quad (1)$$

During muscovite dehydration melting, muscovite is preferentially melted compared with plagioclase. It is accompanied by the growth of peritectic K-feldspar, resulting in a melt with a higher Rb/Sr ratio, lower Sr content, and radiogenic $^{87}Sr/^{86}Sr$ ratio (Harris and Inger, 1992; Patiño Douce and Harris, 1998). It is evidenced by the perfect correlations between $^{87}Sr/^{86}Sr_i$ and Sr ($r^2 = 0.82$), Rb/Sr ratio ($r^2 = 0.99$, **Figures 5A,B**). The $^{87}Sr/^{86}Sr_i$ values of the leucosome increase as the Rb/Sr increases and Sr decreases.

In metasediments, the Sm-Nd system is mainly controlled by apatite and monazite (Rapp et al., 1987). The dissolution of apatite and monazite may play an essential role in shaping the Nd isotopic systematics of anatectic melt (Ayres and Harris, 1997; Zeng et al., 2005). Although Hammerli et al. (2014) argued that metasedimentary rock has reached Nd isotopic equilibrium before 550°C based on *in situ* Sm–Nd isotope study of accessory minerals, we suggest that this scenario does not match with the migmatite in this study. The Nd isotope homogenization between accessory phases in the study of Hammerli et al. (2014) was mainly through recrystallization of detrital accessory minerals. However, if the protolith is dominated by minerals that formed at high-grade metamorphic conditions, prograde metamorphism may not result in significant inter-accessory mineral reactions (Wolf et al., 2019). The migmatite in this study has experienced early Paleozoic metamorphism; therefore, the accessory minerals in the migmatite are difficult to recrystallization during prograde metamorphism.

Zeng et al. (2005) suggested that muscovite dehydration melting occurs at low H_2O activity, which promotes apatite dissolution but inhibits monazite dissolution, resulting in a melt with higher Sm/Nd ratios and more radiogenic Nd isotopic compositions than the source. In **Figure 5C**, it is evident that the leucosome has a higher $^{147}Sm/^{144}Nd$ than the GHC metasedimentary rocks. In addition, the fact that more radiogenic leucosomes in Nd isotope have higher P_2O_5 and lower Th content as well supported the preferable dissolution of apatite during anatexis (**Figures 5E,F**). In the process of crust-mantle differentiation, the crust has higher Rb/Sr and lower Sm/Nd ratios than the mantle. Therefore, the $^{87}Sr/^{86}Sr$ and $^{143}Nd/^{144}Nd$ (or εNd) of terrestrial rocks from various sources are commonly coupled with negative correlation (Clemens et al., 2017). The exceptional example is that the minerals with higher muscovite/plagioclase and apatite/monazite ratios entering the melt during muscovite dehydration melting of metapelite would result in a positive correlation in the Sr-Nd isotope couple, which also occurred in the leucosome (**Figure 5D**).

Since zircon is the primary Hf-bearing mineral in metasedimentary rocks, the Hf isotope of anatectic melt is mainly controlled by the zircon dissolution in the source area (Bea et al., 1994). The variations of Hf isotopes composition in the *in situ* anatectic melt have been attributed to 1) preferential dissolution of uranium-rich zircon (Gao et al., 2021) and 2) disequilibrium melting and peritectic reaction (Farina et al., 2014; Tang et al., 2014; Xia et al., 2022). Gao et al. (2021) reported that the uranium-rich zircons in the Himalayan leucogranite are characterized by higher $\varepsilon Hf_{(t)}$ values. The uranium-rich zircons are preferential entering melt during crust melting because the severe radiation damage reduces their stability (Gao et al., 2021). However, the lack of correlation between U and $\varepsilon Hf_{(t)}$ indicates that the Hf isotope variation in the leucosome is not caused by the preferential dissolution of uranium-rich zircons in the source (**Figure 6D**). The negative correlation between Zr and $\varepsilon Hf_{(t)}$ indicates that the radiogenic Hf isotope in the leucosome was contributed by Zr-poor mineral (**Figure 6E**). With extremely low Lu/Hf ratios, zircon contributes to the unradiogenic Hf, whereas other rock-forming minerals hosting the most Lu contribute to the radiogenic Hf (Tang et al., 2014; Xia et al., 2022). Disequilibrium melting affects retention of unradiogenic Hf in refractory zircon, or release of radiogenic Hf from easily melted minerals, e.g., feldspar and mica, resulting in the melt having a high εHf (the so-called "zircon effect"; Tang et al., 2014). In addition, recent study by *in situ* analyses of zircon in migmatite shows that newly grown zircons have elevation Hf isotope ratios than their protolith zircons (Xia et al., 2022). Xia et al. (2022) attributed to the peritectic reaction of garnet with high Lu/Hf. However, there is no evidence indicates that garnet is involved in the process of muscovite dehydration melting. Hence, we suggest that incomplete dissolution of zircon may contribute to leucosomes with higher εHf. It is supported by the higher $^{176}Lu/^{177}Hf$ ratios in the leucosome than in the source (**Figure 6A**). The trend of Nd-Hf isotopes in the leucosome deviates from the terrestrial array and shows elevated $\varepsilon Hf_{(t)}$ and $\varepsilon Nd_{(t)}$ ratios (**Figure 6B**). In conclusion, we suggest that the incongruent

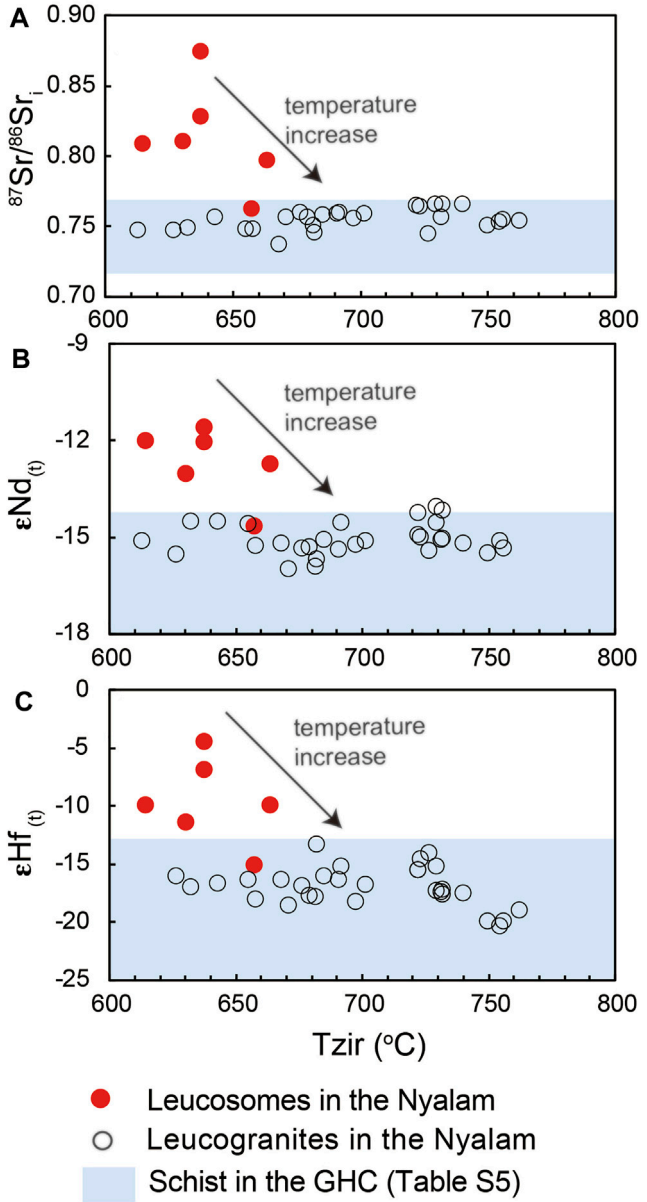

FIGURE 7 | The diagrams show the change of **(A)** $^{87}Sr/^{86}Sri$, **(B)** $\varepsilon Nd_{(t)}$, **(C)** $\varepsilon Hf_{(t)}$ of leucosome and leucogranite with the crystallization temperature. The crystallization temperature was estimated by zircon saturation thermometer (Watson and Harrison, 1983. The blue areas represent the isotope range of the GHC.

trend of Nd-Hf isotopes is resulted from the preferred dissolution of Zr-poor accessory minerals such as mica and feldspar.

5.3 Implications

Based on the zircon saturation thermometer from Watson and Harrison (1983), we estimated the crystallization temperature of the leucosome is 663–614°C, which is consistent with the metamorphism temperature constrained by Wang et al. (2013). The negative correlations between isotopes and crystallization temperatures indicate that temperature has an important effect on the isotopic equilibrium during anatexis (**Figure 7**). It is also supported by the negative correlation between Sr and $^{87}Sr/^{86}Sr_i$ (**Figure 5A**). Because Sr content in the melt increases when melt fraction increases during muscovite dehydration melting of metapelite (Harris and Inger, 1992; Knesel and Davidson, 2002). The leucosome crystallized from higher melt fractions might be produced at higher melting temperatures, has a higher Sr content.

With the temperature increase, the isotopic signature of the leucosome is closer to the source. The rise of temperature during crustal anatexis has three main effects. Firstly, a higher temperature would accelerate the isotopes exchanges, e.g., the diffusion rate of Sr in plagioclase increases exponentially with an increasing temperature (Cherniak and Watson, 1994). Secondly, a higher temperature would prompt the dissolution of accessory minerals because their solubility is a function of temperature (Watson and Harrison, 1983; Montel, 1993). Thirdly, a higher temperature would cause the decomposition of refractory minerals in the metasediments (e.g., biotite and garnet) containing accessory minerals (Bea et al., 2006). These phases are commonly stable under low-degree melting conditions, such as water-saturation melting and muscovite dehydration melting. Therefore, the trapped accessory minerals are difficult to touch the melt to reach an equilibrium.

In conclusion, caution must be taken when using the Sr-Nd-Hf isotopes of low-temperature melt was produced by water-saturated and muscovite dehydration melting to fingerprint the source. The isotopic signatures of high-temperature melt (e.g., the temperature beyond water-saturated and muscovite-dehydration melting) might inherit the isotopic composition of the source more faithfully. It was evidenced by the Nd-Hf isotopic difference between A-type and S-type granite. The Nd-Hf isotopes of S-type granite are deviated from the terrestrial Nd-Hf isotope array compared with A-type granite (Zhang et al., 2020).

The Sr-Nd-Hf disequilibrium revealed by this study has broad implications for the petrogenesis of Himalayan leucogranite. The Himalayan leucogranite might have evolved from a high-temperature magma, which decomposed the biotite, and liberated the accessory minerals to ultimate equilibrium with the melt. The analyzed Sr-Nd-Hf isotopes of leucogranite in the Nyalam present a relatively uniform composition (**Figures 5**, **6**). The $^{87}Sr/^{86}Sr_i$, $\varepsilon Nd_{(t)}$, and $\varepsilon Hf_{(t)}$ of leucogranite do not change with the decreasing crystallization temperature (**Figure 7**). In addition, the $^{87}Sr/^{86}Sr_i$, $\varepsilon Nd_{(t)}$, and $\varepsilon Hf_{(t)}$ of Nyalam leucogranite do not change with the decrease of Sr, P_2O_5, and Zr, indicating that fractional crystallization influences leucogranite composition. The result is consistent with the conclusion of Yang et al. (2019) that the Himalayan leucogranite is the magma produced in the deeper Himalayan orogenic root during peak metamorphism. Subsequently, extensive fractional crystallization occurred through the upward migration of magma along the STDS during the GHC exhumation.

6 CONCLUSION

1) The U-Pb ages of inherited zircon core and Rb-Sr errorchron of the leucosome record an early Paleozoic tectono-thermal

event. Sr-Nd-Hf isotopic homogenization of the leucosome has not been attained during the Himalayan metamorphism.
2) The Sr-Nd-Hf isotopes of the leucosome have a wide range of variations and deviate from the GHC metasediments. During muscovite dehydration melting, preferred consumption of muscovite relative to plagioclase contributed to more radiogenic Sr isotopic compositions in the leucosome, whereas preferable dissolution of apatite and inhibit dissolution of monazite and zircon controlled the less radiogenic Nd-Hf isotopic compositions in the leucosome.
3) The Sr-Nd-Hf isotopic disequilibrium commonly appears in low-temperature partial melting of metasediments. The increase in melting temperature can prompt an isotopic equilibrium between the melt and source.

DATA AVAILABILITY STATEMENT

The original contributions presented in the study are included in the article/**Supplementary Material**, further inquiries can be directed to the corresponding author.

AUTHOR CONTRIBUTIONS

F-YW designed the project. LY, J-MW, X-CL, and F-YW did the fieldwork and collected samples. LY, J-MW, and XL carried out the whole rock Sr-Nd-Hf isotopes analysis. GK carried out the zircon U-Pb dating. All the authors discussed the results and edited the manuscript.

FUNDING

This project received funding from the National Science Foundation of China (Grant number is 41972065, 41888101, and 41772058), the Second comprehensive scientific investigation into Qinghai-Tibet Plateau (Grant number is 2019QZKK0802), and State Key Laboratory of Lithospheric Evolution (E152510201).

ACKNOWLEDGMENTS

We are grateful to Dr. Chao Wang and two anonymous reviewers for their detailed and comprehensive reviews, which improve the quality of the paper significantly.

SUPPLEMENTARY MATERIAL

The Supplementary Material for this article can be found online at: https://www.frontiersin.org/articles/10.3389/feart.2022.891960/full#supplementary-material

REFERENCES

Acosta-Vigil, A., London, D., Morgan, G. B., Cesare, B., Buick, I., Hermann, J., et al. (2017). Primary Crustal Melt Compositions: Insights into the Controls, Mechanisms and Timing of Generation from Kinetics Experiments and Melt Inclusions. *Lithos* 286-287, 454–479. doi:10.1016/j.lithos.2017.05.020

Ayres, M., and Harris, N. (1997). REE Fractionation and Nd-Isotope Disequilibrium during Crustal Anatexis: Constraints from Himalayan Leucogranites. *Chem. Geology.* 139, 249–269. doi:10.1016/S0009-2541(97)00038-7

Bea, F., Montero, P., and Ortega, M. (2006). A LA-ICP-Ms Evaluation of Zr Reservoirs in Common Crustal Rocks: Implications for Zr and Hf Geochemistry, and Zircon-Forming Processes. *Can. Mineral.* 44, 693–714. doi:10.2113/gscanmin.44.3.693

Bea, F., Pereira, M. D., and Stroh, A. (1994). Mineral/leucosome Trace-Element Partitioning in a Peraluminous Migmatite (A Laser Ablation-ICP-MS Study). *Chem. Geology.* 117, 291–312. doi:10.1016/0009-2541(94)90133-3

Brown, C. R., Yakymchuk, C., Brown, M., Fanning, C. M., Korhonen, F. J., Piccoli, P. M., et al. (2016). From Source to Sink: Petrogenesis of Cretaceous Anatectic Granites from the Fosdick Migmatite-Granite Complex, West Antarctica. *J. Pet.* 57, 1241–1278. doi:10.1093/petrology/egw039

Burchfiel, B. C., Zhiliang, C., Hodges, K. V., Yuping, L., Royden, L. H., Changrong, D., et al. (1992). The South Tibetan Detachment System, Himalayan Orogen: Extension Contemporaneous with and Parallel to Shortening in a Collisional Mountain Belt. *Geol. Soc. Am. Spe. Pap.* 269, 1–41. doi:10.1130/SPE269-p1

Cawood, P. A., Johnson, M. R. W., and Nemchin, A. A. (2007). Early Palaeozoic Orogenesis along the Indian Margin of Gondwana: Tectonic Response to Gondwana Assembly. *Earth Planet. Sci. Lett.* 255, 70–84. doi:10.1016/j.epsl.2006.12.006

Chappell, B. W. (1996). Magma Mixing and the Production of Compositional Variation within Granite Suites: Evidence from the Granites of Southeastern Australia. *J. Pet.* 37, 449–470. doi:10.1016/j.epsl.2006.12.00610.1093/petrology/37.3.449

Cherniak, D. J., and Watson, E. B. (1994). A Study of Strontium Diffusion in Plagioclase Using Rutherford Backscattering Spectroscopy. *Geochimica et Cosmochimica Acta* 58, 5179–5190. doi:10.1016/0016-7037(94)90303-410.1016/0016-7037(94)90303-4

Clemens, J. D., Elburg, M. A., and Harris, C. (2017). Origins of Igneous Microgranular Enclaves in Granites: the Example of Central Victoria, Australia. *Contrib. Mineral. Petrol.* 172, 1–27. doi:10.1007/s00410-017-1409-2

DeCelles, P. G., Gehrels, G. E., Quade, J., LaReau, B., and Spurlin, M. (2000). Tectonic Implications of U-Pb Zircon Ages of the Himalayan Orogenic belt in nepal. *Science* 288, 497–499. doi:10.1126/science.288.5465.497

Deniel, C., Vidal, P., Fernandez, A., Le Fort, P., and Peucat, J.-J. (1987). Isotopic Study of the Manaslu Granite (Himalaya, Nepal): Inferences on the Age and Source of Himalayan Leucogranites. *Contr. Mineral. Petrol.* 96, 78–92. doi:10.1007/BF00375529

DePaolo, D. J. (1981). Trace Element and Isotopic Effects of Combined Wallrock Assimilation and Fractional Crystallization. *Earth Planet. Sci. Lett.* 53, 189–202. doi:10.1016/0012-821X(81)90153-9

Farina, F., Stevens, G., Gerdes, A., and Frei, D. (2014). Small-scale Hf Isotopic Variability in the Peninsula Pluton (South Africa): the Processes that Control Inheritance of Source 176Hf/177Hf Diversity in S-type Granites. *Contrib. Mineral. Petrol.* 168, 1065. doi:10.1007/s00410-014-1065-8

Faure, G., and Mensing, T. M. (2005). *Isotopes : Principles and Applications*. Hoboken, NJ: wiley.

Gao, L.-E., Zeng, L., Hu, G., Wang, Y., Wang, Q., Guo, C., et al. (2019). Early Paleozoic Magmatism along the Northern Margin of East Gondwana. *Lithos* 334-335, 25–41. doi:10.1016/j.lithos.2019.03.007

Gao, P., Yakymchuk, C., Zhang, J., Yin, C., Qian, J., and Li, Y. (2021). Preferential Dissolution of Uranium-Rich Zircon Can Bias the Hafnium Isotope Compositions of Granites. *Geology* 50, 336–340. doi:10.1130/G49656.1

Griffin, W. L., Powell, W. J., Pearson, N. J., and O'Reilly, S. Y. (2008). "Glitter: Data Reduction Software for Laser Ablation Icp-Ms," in *Laser Ablation-ICP-MS in the Earth Sciences: Current Practices and Outstanding Issues*. Editor P. J. Sylvester (Mineralogical Association of Canada: Quebec City, QC), 308–311.

Hammerli, J., Kemp, A. I. S., and Spandler, C. (2014). Neodymium Isotope Equilibration during Crustal Metamorphism Revealed by *In Situ* Microanalysis of REE-Rich Accessory Minerals. *Earth Planet. Sci. Lett.* 392, 133–142. doi:10.1016/j.epsl.2014.02.018

Harris, N., and Ayres, M. (1998). The Implications of Sr-Isotope Disequilibrium for Rates of Prograde Metamorphism and Melt Extraction in Anatectic Terrains. *Geol. Soc. Lond. Spec. Publications* 138, 171–182. doi:10.1144/GSL.SP.1996.138.01.10

Harris, N. B. W., and Inger, S. (1992). Trace Element Modelling of Pelite-Derived Granites. *Contr. Mineral. Petrol.* 110, 46–56. doi:10.1007/BF00310881

Inger, S., and Harris, N. (1993). Geochemical Constraints on Leucogranite Magmatism in the Langtang Valley, Nepal Himalaya. *J. Pet.* 34, 345–368. doi:10.1093/petrology/34.2.345

Ji, M., Gao, X.-Y., and Zheng, Y.-F. (2022). Geochemical Evidence for Partial Melting of Progressively Varied Crustal Sources for Leucogranites during the Oligocene-Miocene in the Himalayan Orogen. *Chem. Geology.* 589, 120674. doi:10.1016/j.chemgeo.2021.120674

Ji, W.-Q., Wu, F.-Y., Wang, J.-M., Liu, X.-C., Liu, Z.-C., Zhang, Z., et al. (2020). Early Evolution of Himalayan Orogenic belt and Generation of Middle Eocene Magmatism: Constraint from Haweng Granodiorite Porphyry in the Tethyan Himalaya. *Front. Earth Sci.* 8, 236. doi:10.3389/feart.2020.00236

Kapp, P., and DeCelles, P. G. (2019). Mesozoic-Cenozoic Geological Evolution of the Himalayan-Tibetan Orogen and Working Tectonic Hypotheses. *Am. J. Sci.* 319, 159–254. doi:10.2475/03.2019.01

Knesel, K. M., and Davidson, J. P. (2002). Insights into Collisional Magmatism from Isotopic Fingerprints of Melting Reactions. *Science* 296, 2206–2208. doi:10.1126/science.1070622

Leloup, P. H., Liu, X., Mahéo, G., Paquette, J.-L., Arnaud, N., Aubray, A., et al. (2015). New Constraints on the Timing of Partial Melting and Deformation along the Nyalam Section (central Himalaya): Implications for Extrusion Models. *Geol. Soc. Lond. Spec. Publications* 412, 131–175. doi:10.1144/SP412.11

Linnemann, U., Gerdes, A., Hofmann, M., and Marko, L. (2014). The Cadomian Orogen: Neoproterozoic to Early Cambrian Crustal Growth and Orogenic Zoning along the Periphery of the West African Craton-Constraints from U-Pb Zircon Ages and Hf Isotopes (Schwarzburg Antiform, Germany). *Precambrian Res.* 244, 236–278. doi:10.1016/j.precamres.2013.08.007

Montel, J.-M. (1993). A Model for Monazite/melt Equilibrium and Application to the Generation of Granitic Magmas. *Chem. Geology.* 110, 127–146. doi:10.1016/0009-2541(93)90250-M

Myrow, P. M., Thompson, K. R., Hughes, N. C., Paulsen, T. S., Sell, B. K., and Parcha, S. K. (2006). Cambrian Stratigraphy and Depositional History of the Northern Indian Himalaya, Spiti Valley, north-central India. *Geol. Soc. America Bull.* 118, 491–510. doi:10.1130/B25828.1

Najman, Y., Appel, E., Boudagher-Fadel, M., Bown, P., Carter, A., Garzanti, E., et al. (2010). Timing of India-Asia Collision: Geological, Biostratigraphic, and Palaeomagnetic Constraints. *J. Geophys. Res.* 115, B12. doi:10.1029/2010JB007673

Palin, R. M., Treloar, P. J., Searle, M. P., Wald, T., White, R. W., and Mertz-Kraus, R. (2018). U-pb Monazite Ages from the Pakistan Himalaya Record Pre-himalayan Ordovician Orogeny and Permian continental Breakup. *Geol. Soc. Am. Bull.* 130, 2047–2061. doi:10.1130/B31943.1

Parrish, R. R., and Hodges, V. (1996). Isotopic Constraints on the Age and Provenance of the Lesser and Greater Himalayan Sequences, Nepalese Himalaya. *Geol. Soc. Am. Bull.* 108, 904–911. doi:10.1130/0016-7606(1996)108<0904:icotaa>2.3.co;2

Patino Douce, A. E., and Harris, N. (1998). Experimental Constraints on Himalayan Anatexis. *J. Pet.* 39, 689–710. doi:10.1093/petroj/39.4.689

Rapp, R. P., Ryerson, F. J., and Miller, C. F. (1987). Experimental Evidence Bearing on the Stability of Monazite during Crustal Anaatexis. *Geophys. Res. Lett.* 14, 307–310. doi:10.1029/GL014i003p00307

Robinson, D. M., DeCelles, P. G., Patchett, P. J., and Garzione, C. N. (2001). The Kinematic Evolution of the Nepalese Himalaya Interpreted from Nd Isotopes. *Earth Planet. Sci. Lett.* 192, 507–521. doi:10.1016/S0012-821X(01)00451-4

Rudnick, R. L., and Gao, S. (2003). "Composition of the continental Crust," in *Treatise on Geochemistry*. Editor R. L. Rudnick (Amsterdam: Elsevier), 3, 1–64. doi:10.1016/b0-08-043751-6/03016-4

Spencer, C. J., Dyck, B., Mottram, C. M., Roberts, N. M. W., Yao, W.-H., and Martin, E. L. (2019). Deconvolving the Pre-himalayan Indian Margin - Tales of Crustal Growth and Destruction. *Geosci. Front.* 10, 863–872. doi:10.1016/j.gsf.2018.02.007

Tang, M., Wang, X.-L., Shu, X.-J., Wang, D., Yang, T., and Gopon, P. (2014). Hafnium Isotopic Heterogeneity in Zircons from Granitic Rocks: Geochemical Evaluation and Modeling of "Zircon Effect" in Crustal Anatexis. *Earth Planet. Sci. Lett.* 389, 188–199. doi:10.1016/j.epsl.2013.12.036

Taylor, J., Nicoli, G., Stevens, G., Frei, D., and Moyen, J.-F. (2014). The Processes that Control Leucosome Compositions in Metasedimentary Granulites: Perspectives from the Southern Marginal Zone Migmatites, Limpopo Belt, South Africa. *J. Meta. Geol.* 32, 713–742. doi:10.1111/jmg.12087

Vervoort, J. D., Plank, T., and Prytulak, J. (2011). The Hf-Nd Isotopic Composition of marine Sediments. *Geochimica et Cosmochimica Acta* 75, 5903–5926. doi:10.1016/j.gca.2011.07.046

Wang, J.-M., Wu, F.-Y., Rubatto, D., Liu, S.-R., Zhang, J.-J., Liu, X.-C., et al. (2017). Monazite Behaviour during Isothermal Decompression in Pelitic Granulites: a Case Study from Dinggye, Tibetan Himalaya. *Contrib. Mineral. Petrol.* 172, 1–30. doi:10.1007/s00410-017-1400-y

Wang, J.-M., Zhang, J.-J., Liu, K., Zhang, B., Wang, X.-X., Rai, S., et al. (2016). Spatial and Temporal Evolution of Tectonometamorphic Discontinuities in the central Himalaya: Constraints from P-T Paths and Geochronology. *Tectonophysics* 679, 41–60. doi:10.1016/j.tecto.2016.04.035

Wang, J. M., Zhang, J. J., and Wang, X. X. (2013). Structural Kinematics, Metamorphic P-T Profiles and Zircon Geochronology across the Greater Himalayan Crystalline Complex in South-central Tibet: Implication for a Revised Channel Flow. *J. Meta. Geol.* 31, 607–628. doi:10.1111/jmg.12036

Wang, J., Zhang, J., Wei, C., Rai, S., Wang, M., and Qian, J. (2015). Characterising the Metamorphic Discontinuity across the Main Central Thrust Zone of Eastern-central Nepal. *J. Asian Earth Sci.* 101, 83–100. doi:10.1016/j.jseaes.2015.01.027

Wang, X., Zhang, J., Santosh, M., Liu, J., Yan, S., and Guo, L. (2012). Andean-type Orogeny in the Himalayas of South Tibet: Implications for Early Paleozoic Tectonics along the Indian Margin of Gondwana. *Lithos* 154, 248–262. doi:10.1016/j.lithos.2012.07.011

Watson, E. B., and Harrison, T. M. (1983). Zircon Saturation Revisited: Temperature and Composition Effects in a Variety of Crustal Magma Types. *Earth Planet. Sci. Lett.* 64, 295–304. doi:10.1016/0012-821X(83)90211-X

Weinberg, R. F. (2016). Himalayan Leucogranites and Migmatites: Nature, Timing and Duration of Anatexis. *J. Metamorph. Geol.* 34, 821–843. doi:10.1111/jmg.12204

Weis, D., Kieffer, B., Hanano, D., Nobre Silva, I., Barling, J., Pretorius, W., et al. (2007). Hf Isotope Compositions of U.S. Geological Survey Reference Materials. *Geochem. Geophys. Geosyst.* 8, a–n. doi:10.1029/2006GC001473

Weis, D., Kieffer, B., Maerschalk, C., Barling, J., De Jong, J., Williams, G. A., et al. (2006). High-precision Isotopic Characterization of USGS Reference Materials by TIMS and MC-ICP-MS. *Geochem. Geophys. Geosyst.* 7, a–n. doi:10.1029/2006GC001283

Whitney, D. L., and Evans, B. W. (2010). Abbreviations for Names of Rock-Forming Minerals. *Am. Mineral.* 95, 185–187. doi:10.2138/am.2010.3371

Wolf, M., Romer, R. L., and Glodny, J. (2019). Isotope Disequilibrium during Partial Melting of Metasedimentary Rocks. *Geochimica et Cosmochimica Acta* 257, 163–183. doi:10.1016/j.gca.2019.05.008

Wu, F.-Y., Ji, W.-Q., Wang, J.-G., Liu, C.-Z., Chung, S.-L., and Clift, P. D. (2014). Zircon U-Pb and Hf Isotopic Constraints on the Onset Time of India-Asia Collision. *Am. J. Sci.* 314, 548–579. doi:10.2475/02.2014.04

Wu, F.-Y., Liu, X.-C., Liu, Z.-C., Wang, R.-C., Xie, L., Wang, J.-M., et al. (2020). Highly Fractionated Himalayan Leucogranites and Associated Rare-Metal Mineralization. *Lithos* 352-353, 105319. doi:10.1016/j.lithos.2019.105319

Xia, Q.-X., Chen, Y.-X., Chen, R.-X., and Zheng, Y.-F. (2022). Elevation of Zircon Hf Isotope Ratios during Crustal Anatexis: Evidence from Migmatites Close to the Eastern Himalayan Syntaxis in southeastern Tibet. *Lithos* 412-413, 106592. doi:10.1016/j.lithos.2022.106592

Xie, L., Zhang, Y., Zhang, H., Sun, J., and Wu, F. (2008). *In Situ* simultaneous Determination of Trace Elements, U-Pb and Lu-Hf Isotopes in Zircon and Baddeleyite. *Sci. Bull.* 53, 1565–1573. doi:10.1007/s11434-008-0086-y

Yang, L., Liu, X.-C., Wang, J.-M., and Wu, F.-Y. (2019). Is Himalayan Leucogranite a Product by *In Situ* Partial Melting of the Greater Himalayan Crystalline? A Comparative Study of Leucosome and Leucogranite from Nyalam, Southern Tibet. *Lithos* 342-343, 542–556. doi:10.1016/j.lithos.2019.06.007

Zeng, L., Asimow, P. D., and Saleeby, J. B. (2005). Coupling of Anatectic Reactions and Dissolution of Accessory Phases and the Sr and Nd Isotope Systematics of Anatectic Melts from a Metasedimentary Source. *Geochimica et Cosmochimica Acta* 69, 3671–3682. doi:10.1016/j.gca.2005.02.035

Zhang, C., Liu, D., Zhang, X., Spencer, C., Tang, M., Zeng, J., et al. (2020). Hafnium Isotopic Disequilibrium during Sediment Melting and Assimilations. *Geochem. Persp. Let.* 12, 34–39. doi:10.7185/geochemlet.2001

Conflict of Interest: The authors declare that the research was conducted in the absence of any commercial or financial relationships that could be construed as a potential conflict of interest.